Nano Research

Open Access

Research Article

Bright and stable quantum confined $CsPbBr_3$ nanocrystals through post-synthetic chemical cutting and *in-situ* encapsulation

Hao Zhang, Jiang Chen, Tiantian Zhu, Rui Wang, Xuemei Wang, Xijun Xu, and Jianli Wang ✉

College of Chemical Engineering, Zhejiang University of Technology, Hangzhou 310014, China

Cite this article: *Nano Research*, **2025**, *18*, 94907131. https://doi.org/10.26599/NR.2025.94907131

ABSTRACT: Quantum-confined $CsPbBr_3$ nanocrystals are promising cyan/blue-emitting materials with exceptional potential for advanced lighting and display technologies. However, their practical application is often limited by low luminescent efficiency, undesirable color purity and instability stemming from inadequate size uniformity, and high surface defect density. Here, we propose a post-synthetic chemical cutting and *in-situ* encapsulation approach using 3-aminopropyltriethoxysilane (APTES) combined with polymethylhydrosiloxane (PMHS) to synthesize and stabilize $CsPbBr_3$ nanocrystals with significant quantum confinement. APTES can function as a chemical scissor efficiently cutting the green emitting $CsPbBr_3$ (9.8 nm) to smaller counterparts (3.9–7.9 nm), while also passivating surface defects through A-site doping. Crosslinking between APTES and PMHS prevents phase transformation during synthesis and forms a polymeric network that encapsulates and separates the quantum confined $CsPbBr_3$. The resulting composites exhibit tunable emission from 517 to 461 nm, a narrow linewidth of approximately 15 nm, and quantum yields over 80%. Moreover, incorporating one $CsPbBr_3$ composite into a white light-emitting diode to fill the "cyan gap" significantly enhances the color rendering index from 77.7 to 86.4. This work provides an effective strategy for developing bright and stable quantum-confined $CsPbBr_3$ for advanced lighting applications.

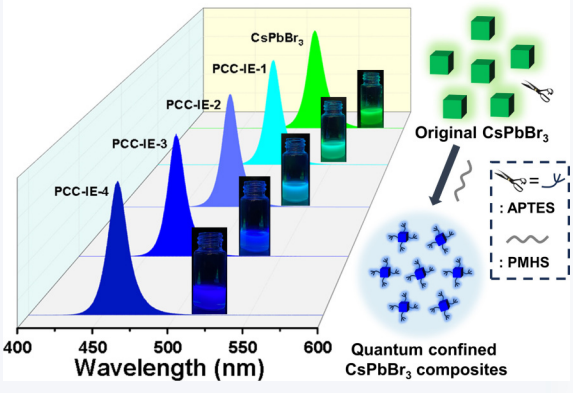

KEYWORDS: perovskite nanocrystal, $CsPbBr_3$, quantum confinement, luminescent efficiency, stability

1 Introduction

In recent years, all-inorganic perovskite nanocrystals ($CsPbX_3$, X = Cl, Br, I) have emerged as an exciting class of colloid semiconductors that possess many desirable features for optoelectronic applications, such as high photoluminescent quantum yield (PLQY), good emission purity, broad emission range as well as low material costs [1–4]. To date, much endeavour has been devoted to synthesize all-inorganic nanocrystals (NCs) with stable green or red fluorescence emission (typically $CsPbBr_3$ and $CsPbI_3$), successfully boosting their PLQY to near unity [5, 6]. However, the exploitation of perovskite NCs with bright and stable cyan/blue emitting is apparently lagging behind [7, 8]. To achieve some advanced light emitting applications like full spectrum lighting, underwater communication, and full color display [9, 10], cyan/blue emitting components are indispensable. Thus, developing cyan/blue emitting counterparts with simultaneously high PLQY and stability is crucial for promoting extensive application of all-inorganic perovskite NCs.

Composition engineering is the most widely employed approach to obtain cyan/blue emitting perovskite NCs by controlling the Cl/Br ratio in $CsPbCl_xBr_{3-x}$ or through B-site doping in $CsPbBr_3$ [11–13]. Nevertheless, the resulting mixed ion perovskite NCs are susceptible to phase separation under optical or electric fields, which usually leads to undesirable spectral shift [14–17]. Tuning photoluminescence of $CsPbBr_3$ via strong quantum confinement effect offers another route to realize cyan/blue fluorescence emission. Specifically, at least one dimension of the $CsPbBr_3$ nanoparticle must be reduced to a scale below its Bohr exciton radius [18]. Based on this, several ultrasmall $CsPbBr_3$ quantum dots, $CsPbBr_3$ nanoplates or nanosheets with cyan/blue emission have been reported in previous studies [19, 20]. However, preparing strongly quantum confined $CsPbBr_3$ nanoparticles with a uniform size distribution is challenging due to their pronounced ionicity and low formation energy, which typically leads to multi-peak

Received: September 20, 2024; **Revised:** November 6, 2024
Accepted: November 12, 2024

✉Address correspondence to wangjl@zjut.edu.cn

photoluminescence profiles [21]. Besides, these quantum confined perovskite NCs normally suffer from low PLQY and poor stability because of high proportion of surface defects and large surface-to-volume ratio [22, 23]. Despite PLQY could be improved by surface passivation or ligand engineering [24, 25], the stability issue still persists. The strongly quantum confined $CsPbBr_3$ particles are prone to aggregation due to their large surface energy, resulting in unstable emission color. In order to achieve bright and stable cyan/blue emission, proper matrices should be selected to restrict the self-aggregation of the strongly quantum confined perovskite NCs as well as protect them against ambient stimulus like polar molecules, heat, and light [26, 27]. For instance, Xiao et al. designed a polymer ligand with adjacent amide and carboxylic acid groups, as well as double bonds, which induced a significant blue shift in spectra of perovskite NCs. Encapsulating the NCs in polystyrene through crosslinking produced a water-resistant composite [28].

Recently, porous materials including mesoporous silica, molecular sieves, and mesoporous alumina were demonstrated as suitable candidates to *in-situ* grow and stabilize quantum confined $CsPbBr_3$ with cyan/blue fluorescence emission [29–31]. The independent nano-spaces within the porous matrix serve as templates that limit and separate the growth of perovskite nanoparticles, ensuring consistent quantum confinement effects. For instance, Yamauchi and coworkers reported on blue-emitting $CsPbBr_3$ NCs with size of 3.1 nm synthesized by confined growth in mesoporous silica [30]. The mesoporous silica matrix was also found to protect the optical properties of $CsPbBr_3$ from atmospheric conditions. Yu et al. proposed a high temperature evaporation synthesis method to introduce $CsPbBr_3$ nanoparticles into a zeolite framework, achieving accurate size regulation from 2 to 6 nm, associated with tunable fluorescence emissions from 468 to 508 nm [31]. Subsequent amino acid passivation and silane restoration further improved the luminescent efficiency and inhibited crystal merging triggered by water vapor. However, these porous templates are usually acquired by high temperature calcination (over 500 °C), which renders the preparation of quantum confined $CsPbBr_3$ nanocrystals costly. Moreover, the porous structure is troublesome for long-term resisting the penetration of polar molecules [32].

Here, we report a facile post-synthetic chemical cutting and *in-situ* encapsulation (PCC-IE) strategy for the synthesis and stabilization of strongly quantum confined $CsPbBr_3$ NCs at room temperature, employing an amine containing siloxane, 3-aminopropyltriethoxysilane (APTES), in conjugation with polymethylhydrosiloxane (PMHS). Where APTES serves as both a crystal structure modifying agent, efficiently cutting the green emitting $CsPbBr_3$ (9.8 nm) to smaller counterparts (3.9–7.9 nm) with good size and shape uniformity, and a passivator, mitigating surface defects through A-site doping, thus successfully achieving pure cyan/blue emission with high luminescent efficiency (PLQY over 80%). Furthermore, the crosslinking between APTES and PMHS not only averts phase transformation of the quantum confined $CsPbBr_3$ NCs during synthesis, but also *in-situ* establishes a polymeric network that encapsulates and separates the NCs, significantly enhancing their stability against polar solvents, heat, and light. Finally, one of the quantum confined $CsPbBr_3$ composites was applied to supplement the cyan light and alleviate blue light overshoot of a white light-emitting diode (WLED), which improved the color rendering index from 77.7 to 86.4, showing promising potential in full spectrum lighting.

2 Results and discussion

The preparation and stabilization of the strongly quantum confined $CsPbBr_3$ NCs are illustrated in Fig. 1(a). Firstly, the pristine $CsPbBr_3$ NCs were synthesized using the traditional hot-injection method [33]. Then, APTES and PMHS were successively added into the pristine $CsPbBr_3$ NCs solution. Owing to its strong binding affinity for metal halide perovskite materials, APTES quickly anchored to the surface of the $CsPbBr_3$ NCs via ligand exchange [34, 35]. Notably, the amount of APTES added was in significant excess (n_{APTES}/n_{Pb} = 20–70). Typically, such an excess of amine-containing

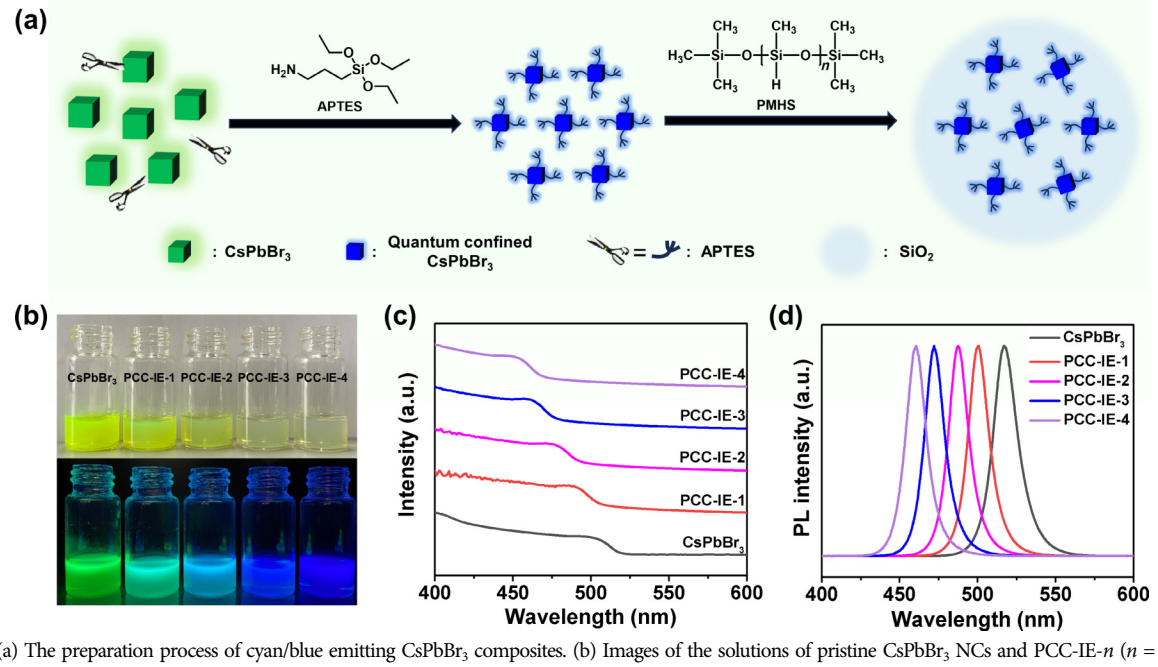

Figure 1 (a) The preparation process of cyan/blue emitting $CsPbBr_3$ composites. (b) Images of the solutions of pristine $CsPbBr_3$ NCs and PCC-IE-*n* (*n* = 1–4) under daylight and 365 nm UV light irradiation. (c) UV–Vis absorption and (d) PL spectra of the pristine $CsPbBr_3$ NCs and PCC-IE-*n* (*n* = 1–4).

ligands would quickly decompose the structure of perovskite NCs, leading to prominent weakening or even total disappearance of photoluminescence [36, 37]. Surprisingly, the APTES ligands didn't immediately destroy the crystal structure of the pristine $CsPbBr_3$ NCs. Instead, they rapidly cut the NCs to metastable counterparts with smaller sizes, resulting in a strong quantum confinement effect, as discussed below. Meanwhile, the terminal ethoxylsilane groups of APTES could go through hydrolysis reaction with the assistance of trace water in the solvent and ambient air (Eq. S1 in the Electronic Supplementary Material (ESM)), forming Si–OH [38, 39]. Afterwards, the –Si–H groups of PMHS chains react with –Si–OH units on the surface of the quantum confined $CsPbBr_3$ NCs (Eq. S2 in the ESM) [40], *in situ* forming an encapsulation layer that stabilizes the strongly quantum confined $CsPbBr_3$ NCs. The samples prepared using the PCC-IE method, with progressively increasing amounts of APTES added, are denoted as PCC-IE-*n* (n = 1–4), respectively. Detail synthesis procedure is provided in the ESM.

As shown in Fig. 1(b), the solutions of pristine $CsPbBr_3$ NCs present bright green fluorescence under 365 nm ultraviolet (UV) light irradiation. With the addition of APTES and PMHS, the solution color of $CsPbBr_3$ NCs under daylight gradually becomes pale, and the corresponding luminescence turns from green to cyan and further to blue. After centrifugation, washing, and vacuum drying, $CsPbBr_3$ composite powders with different emission color could be obtained (Fig. S1 in the ESM). The ultraviolet–visible (UV–Vis) absorption and photoluminescence (PL) spectra of the pristine $CsPbBr_3$ NCs and $CsPbBr_3$ composites are depicted in Figs. 1(c) and 1(d). Compared to pristine $CsPbBr_3$ NCs, the absorption onset of the $CsPbBr_3$ composites exhibits obvious blue-shift, suggesting the formation of $CsPbBr_3$ NCs with strong quantum constraints. Correspondingly, the PL peaks are blue-shifted from 517 to 461 nm. Intriguingly, the full width at half maxima (FWHM) of the emission peaks also declines from 18.3 to around 15.0 nm (Table 1), and no shoulder peak could be detected, indicating that the size of the $CsPbBr_3$ NCs becomes more uniform after the chemical cutting and encapsulation process. During the cutting step, some small fragments might be exfoliated from the pristine $CsPbBr_3$ NCs, which could reassemble to larger grains and finally reach a dynamic balance state. The reassembling processes are benefit for the formation of NCs with more uniform size [28]. The PLQY values of PCC-IE-*n* (n = 1–4) are 83.6%, 83.2%, 82.9%, and 80.5%, respectively. The decrease in PLQY can be attributed to the increase in surface defects or trap states, likely introduced by larger surface-to-volume ratio of smaller $CsPbBr_3$ NCs [3, 22]. Nevertheless, the PLQY values of PCC-IE- n (n = 1–4) are still much superior than most of the cyan/blue emitting $CsPbBr_3$ NCs reported in literatures [31]. However, when larger amount of APTES were added (n_{APTES}/n_{Pb} = 80), the photoluminescence becomes extremely weak (Fig. S2 in the ESM), which might be attributed to partial decomposition of the perovskite structure. Besides, we measured the time-resolved photoluminescence (TRPL) curves of the pristine $CsPbBr_3$ and the quantum confined $CsPbBr_3$ composites (Fig. S3 in the ESM). The PL decay curve of pristine $CsPbBr_3$ is well fitted with a biexponential function, yielding an average PL lifetime (τ_{ave}) of 9.77 ns, whereas those of the PCC-IE-*n* (n = 1–4) samples are better presented by a triexponential mode (Table S1 in the ESM), suggesting more complex relaxation pathways. The extended tail observed in the PL decay of PCC-IE-1 is indicative of exciton trapping and de-trapping from deep trap states [41]. With the addition of APTES, the τ_{ave} of PCC-IE-*n* (n = 1–4) progressively decreased to 6.33 ns, probably due to enhanced quantum confinement effects resulting from the reduced particle size of the $CsPbBr_3$ component [42]. The increased quantum confinement can accelerate radiative recombination processes, which may partly compensate for non-radiative losses induced by surface defects.

Table 1 The PL peak wavelength, FWHM, and PLQY values of $CsPbBr_3$ and PCC-IE-*n* (n = 1–4)

Sample	PL peak (nm)	FWHM (nm)	PLQY (%)
$CsPbBr_3$	517	18.3	86.3
PCC-IE-1	501	15.7	83.6
PCC-IE -2	488	15.4	83.2
PCC-IE -3	472	15.0	82.9
PCC-IE -4	461	15.5	80.5

The structure properties of the quantum confined $CsPbBr_3$ composites were examined by X-ray diffraction (XRD). As shown in Fig. 2(a), the diffraction patterns of the pristine $CsPbBr_3$ NCs match well with the cubic phase $CsPbBr_3$ (PDF#75-0412). The diffraction peaks located at 14.97°, 21.19°, 30.08°, 33.81°, 36.96°, and 43.24° can be assigned to (100), (110), (200), (210), (211), and (220) crystal planes, respectively [43]. These diffraction peaks are preserved in the XRD patterns of PCC-IE-*n* (n = 1–4), demonstrating that the $CsPbBr_3$ phase still exists after the PCC-IE process. The broad bands over 15°–25° are associated with the scattering of amorphous silica [38]. Nevertheless, in the XRD patterns of PCC-IE-*n* (n = 1–4), the characteristic peaks of $CsPbBr_3$ shifted to higher diffraction angles, suggesting the contraction of crystal lattices [44]. Moreover, the diffraction peaks of the quantum confined $CsPbBr_3$ composites PCC-IE-*n* (n = 1–4) are wider than those of the pristine $CsPbBr_3$ NCs. Specifically, the fitted FWHM values of the (200) peaks for PCC-IE-*n* (n = 1–4) display a decreasing trend (Table S2 in the ESM). This implies that the average nanocrystalline size diminishes with increasing amounts of APTES. Besides, the relative intensity of (100) and (200) planes becomes weaker, whereas that of the (110) plane becomes much stronger, implying the pristine $CsPbBr_3$ NCs undergo a chemical cutting process [28].

The composition of the samples was also analysed by Fourier transform infrared (FTIR) spectroscopy (Fig. S4 in the ESM). The pristine $CsPbBr_3$ presents two characteristic peaks at 2922.7 and 2860.5 cm^{-1}, corresponding to the C–H asymmetric and symmetric stretching vibrations of oleic acid (OA) and oleylamine (OAm) [45]. These peaks are significantly weakened in the FTIR spectra of typical quantum confined $CsPbBr_3$ composites due to ligand exchange and polymer matrix encapsulation. The vibration peaks emerged at 1262.1 and 1012.0 cm^{-1} could be assigned to Si–CH_2 and Si–O–C respectively [40], verifying the existence of APTES in the composite samples. Moreover, the characteristic peaks related to Si–H (2174.2 cm^{-1}), Si–O–Si (1116.1 and 753.0 cm^{-1}), and Si–OH (898.2 cm^{-1}) are detected, which demonstrate that the terminal ethoxylsilane groups of APTES undergo a hydrolysis process and condensation with PMHS, forming a silica network [46], as is in accordance with the XRD results.

The transmission electron microscopy (TEM) images of the pristine $CsPbBr_3$ NCs and PCC-IE-*n* (n = 1–4) were shown in Fig. S5 in the ESM and Figs. 2(b)–2(e). The pristine $CsPbBr_3$ displays a cubic shape morphology with an average particle size of 9.8 nm. For PCC-IE-*n* (n = 1–4), it can be clearly observed that the perovskite

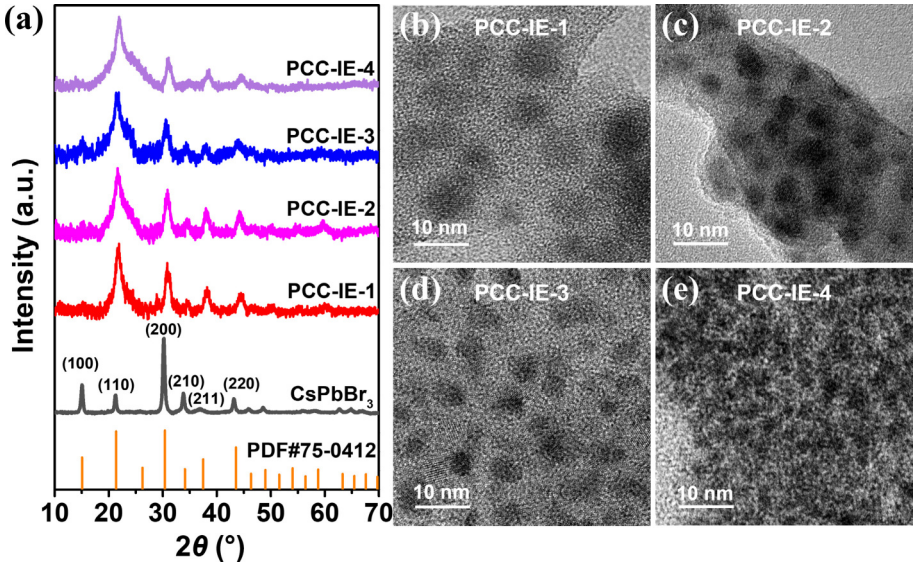

Figure 2 (a) XRD patterns of the pristine $CsPbBr_3$ NCs and PCC-IE-*n* (*n* = 1–4). (b) TEM images of PCC-IE-*n* (*n* = 1–4).

nanocrystals (dark dots) are successfully wrapped with polymer matrix (lighter-colored shell). In addition, the average crystal size declined to 7.9, 5.0, 4.7, and 3.9 nm, respectively (Fig. S6 in the ESM), in consistent with the variation of UV–Vis absorption and PL spectra. High-resolution TEM (HRTEM) images of PCC-IE-*n* (*n* = 1–4) show a lattice distance of 0.2967, 0.2953, 0.2944, and 0.2921 nm, respectively, corresponding to the (200) crystal planes of cubic $CsPbBr_3$ (Fig. S7 in the ESM). The gradually decreased lattice distance also implies the lattice contraction [47]. The energy-dispersive X-ray spectroscopy (EDX) mapping images of the typical composite PCC-IE-3 are shown in Fig. S8 in the ESM. The Cs, Pb, and Br elements were concentrated in the crystalline region, whereas Si, O, and N elements were distributed over the whole region, which also indicates that the perovskite nanocrystals are well encapsulated by the outer polymer shell.

To further elucidate the roles of APTES and PMHS in the preparation of strongly quantum confined $CsPbBr_3$ composites, each of them was individually added to the pristine $CsPbBr_3$ nanocrystal solution. In the absence of PMHS, a blue shift is still observed (within 1 s), highlighting the role of APTES in fast diminishing the size of pristine $CsPbBr_3$ NCs (Fig. S9 in the ESM). Nevertheless, upon exposure to ambient air, the sample begins to flocculate and settle after 30 min, and the resulting composite material quickly degrades into a non-luminescent white powder (Fig. S10 in the ESM). XRD analysis of the white powder reveals that the majority of $CsPbBr_3$ has been converted to non-emissive Cs_4PbBr_6 (Fig. S11 in the ESM), indicating that the quantum confined $CsPbBr_3$ NCs generated through APTES mediated chemical cutting are metastable. This instability is likely caused by the hydrolysis and condensation of excess APTES, which produces a large quantity of polar molecules, triggering the phase transformation of $CsPbBr_3$. The disappearance of PL emission in the generated Cs_4PbBr_6 may be attributed to the absence of defects or impurity phases that act as emission centers [48]. Conversely, without APTES, the PL peak position exhibits minimal shift (Fig. S12 in the ESM), suggesting that PMHS has a negligible effect on size reduction of the pristine $CsPbBr_3$ NCs. However, the addition of PMHS is essential for stabilization of the strongly quantum confined $CsPbBr_3$ NCs. This stabilization effect is due to the reaction between PMHS and APTES, which primarily releases nonpolar hydrogen gas. The reaction proceeds at a faster rate than the self-condensation of APTES, thereby minimizing the formation of polar byproducts. Furthermore, this reaction facilitates the rapid development of a polymeric network that effectively encapsulates and shields the quantum-confined $CsPbBr_3$ NCs from external stimulus, such as moisture.

Above characterizations collective demonstrate that the post-synthetic chemical cutting and *in-situ* encapsulation are effective approach for preparing strongly quantum confined $CsPbBr_3$ composites with tunable emission as well as high color purity. In this process, APTES acts as a crystal structure tailoring agent, rapidly cutting the pristine $CsPbBr_3$ NCs to smaller counterparts with good size and shape uniformity, while PMHS acts as a protective barrier preventing phase transformation of $CsPbBr_3$.

In order to gain more insight into the chemical interaction between APTES and the quantum confined $CsPbBr_3$ NCs, X-ray photoelectron spectroscopy (XPS) studies were conducted. The full scan spectra of the typical samples are shown in Fig. 3(a), which identify the presence of Cs, Pb, Br, Si, N, and O elements on the $CsPbBr_3$ composites. No peak related to Cl could be detected, excluding the possibility of unintentional introduction of Cl ions during sample preparation. This further reveal that the spectra blue shift was induced by quantum confinement effect instead of component engineering. In comparison to that of the pristine $CsPbBr_3$, the peak intensity of Cs, Pb and Br elements for PCC-IE-1 and PCC-IE-3 dramatically reduced, while the O peak intensity prominently increased due to encapsulation of the perovskite nanocrystals by silica shell. Figures 3(b)–3(d) depict the high-resolution XPS spectra of Cs 3d, Pb 4f, and Br 3d. The Cs $3d_{3/2}$ and Cs $3d_{5/2}$ peaks of the pristine $CsPbBr_3$ NCs locate at binding energies of 724.65 and 738.58 eV, respectively, and exhibit little change after the PCC-IE process. The slightly broadening of these peaks are due to decreased signal intensity, which also could be observed for Pb 4f core levels [49]. Differently, the Pb 4f core levels of PCC-IE-1 and PCC-IE-3 both shift to higher binding energies for about 0.21 and 0.26 eV compared to that of the pristine sample. The Br 3d core level of the pristine sample can be deconvoluted into two sub peaks at 68.01 and 69.03 eV, corresponding to Br $3d_{3/2}$

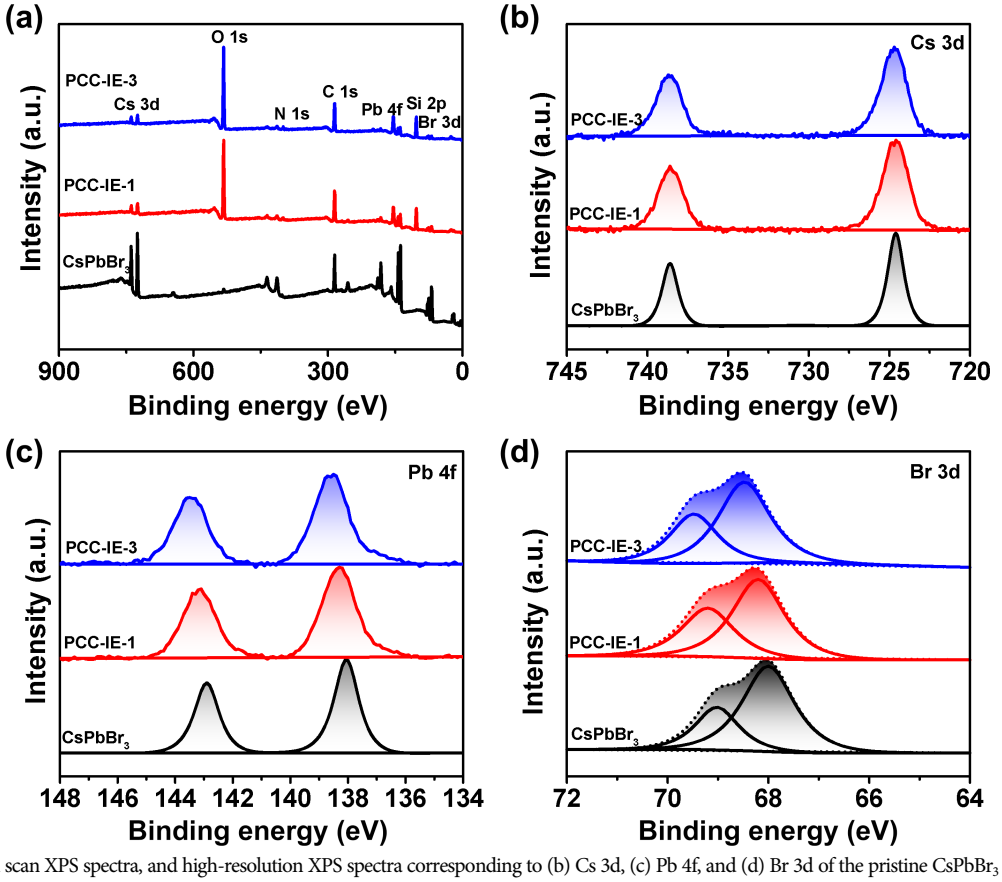

Figure 3 (a) The full scan XPS spectra, and high-resolution XPS spectra corresponding to (b) Cs 3d, (c) Pb 4f, and (d) Br 3d of the pristine $CsPbBr_3$ and typical quantum confined $CsPbBr_3$ composites of PCC-IE-1 and PCC-IE-3.

and Br $3d_{5/2}$, respectively. Intriguingly, these peaks also shift to higher binding energies with increasing addition amount of APTES, in accordance with the Pb 4f peaks, indicating that APTES has a strong interaction with the $PbBr_4^{2-}$ octahedron [50, 51]. For both PCC-IE-1 and PCC-IE-3, the N 1s signal can be deconvoluted into two peak components (Fig. S13 in the ESM). The peak with a lower binding energy originates from the amine groups ($-NH_2$) on APTES, whereas the peaks at higher binding energy (about 401.81 eV) are assigned to protonated amine groups ($-NH_3^+$). We speculate that some APTES molecules were protonated during the post synthetic chemical cutting process, which act as the A-site doping agent for $CsPbBr_3$. According to previous studies, A-site doping of $CsPbBr_3$ nanocrystals by protonated APTES would cause lattice contraction [47], in line with the XRD and TEM observations discussed above. The A-site doping is also benefiting for defect healing [52], accounting for high PLQY of these strongly quantum confined $CsPbBr_3$ composites.

Apart from photoluminescent properties, the stability of the $CsPbBr_3$ composites is also crucial for their practical applications. Normally, metal halide perovskite materials are unstable towards polar solvents due to their ionic nature [53]. To evaluate the polar solvent tolerance of the $CsPbBr_3$ composites, we dispersed them in dimethylformamide (DMF) and ethanol using ultrasonication. The pristine $CsPbBr_3$ was utilized as a contrast group. After ultrasound treatment for 5 min, the photoluminescence of the pristine $CsPbBr_3$ NCs almost totally disappeared, implying structure degradation. In comparison, PCC-IE-*n* (*n* = 1–4) all maintain bright cyan/blue luminescence under UV lamp, and remain over 89% of the initial PL intensity even after 3 months (Figs. 4(a) and 4(b)). The significantly improved polar solvent tolerance of $CsPbBr_3$ composites can be attributed to the existence of outer polymer shell, which hinders the permeation of solvent molecules to inner $CsPbBr_3$ core [54].

Thermostability of the pristine $CsPbBr_3$ and PCC-IE-*n* (*n* = 1–4) were compared by storing the samples at 70 °C (Fig. 4(c) and Fig. S14 in the ESM). After 5 days, the emission intensity of the pristine sample dropped sharply to 3% of its initial value, accompanied by slight red shift in the PL peak. This could be explained by the highly dynamic binding of OA and OAm to perovskite nanocrystals surface [55]. The ligands are more labile at elevated temperature, which leads to increased defect sites. However, during the same aging time, the $CsPbBr_3$ composites PCC-IE-*n* (*n* = 1–4) kept 70%, 67%, 76%, and 72% of the original PL intensity, respectively, with little change of the PL peak position. Moreover, to assess the $CsPbBr_3$ composites' resistance to prolonged light exposure, the samples were subjected to UV light (365 nm, 24 W), and their PL spectra were monitored over time. As shown in Fig. 4(d) and Fig. S15 in the ESM, the relative intensity of the pristine $CsPbBr_3$ quickly decayed to 8% within 5 days, and the PL peak exhibits an obvious red shift for about 12 nm, indicating aggregation of the $CsPbBr_3$ nanocrystals due to light-induced ligand shedding [56]. In contrast, the $CsPbBr_3$ composites PCC-IE-*n* (*n* = 1–4) still retain 57%, 61%, 70%, and 74% of their initial PL intensity, respectively, demonstrating superior photostability. The enhanced thermal resistance and photostability of the $CsPbBr_3$ composites relative to the pristine $CsPbBr_3$ can be assigned to the stronger bonding of APTES to perovskite nanocrystals than that of OA and OAm, as well as the protective encapsulation provided by the polymer

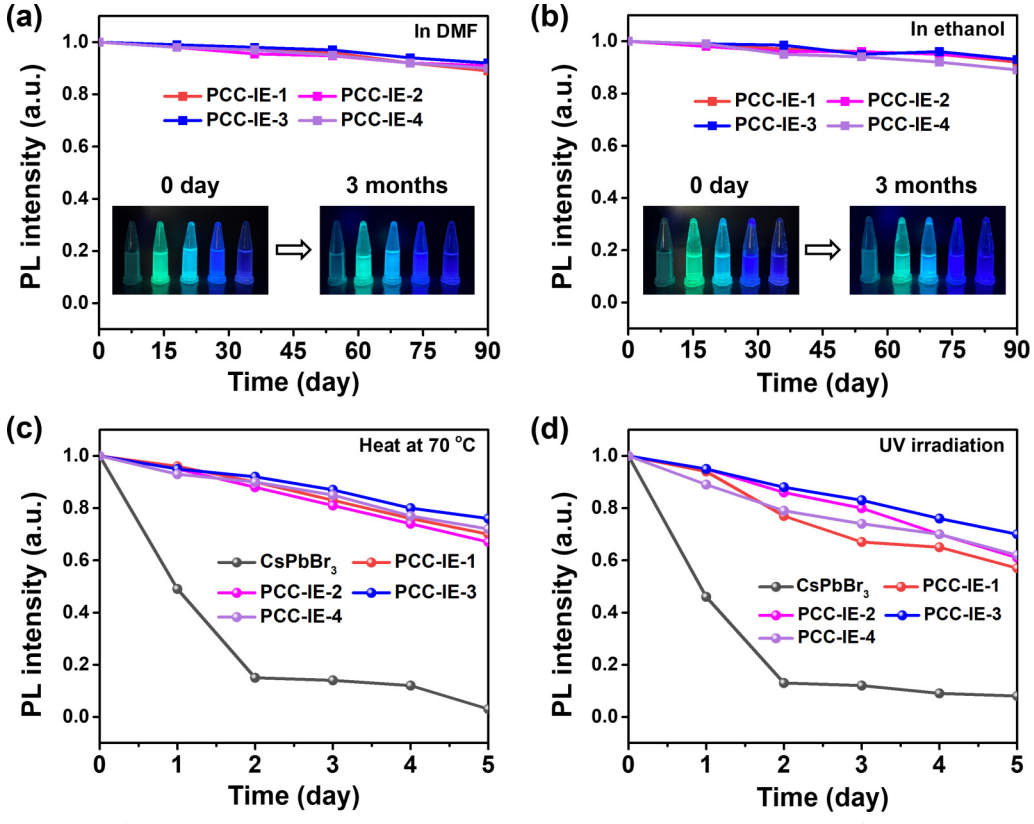

Figure 4 PL intensity evolution of PCC-IE-*n* (*n* = 1–4) in (a) DMF and (b) ethanol (the insets show the solvent tolerance tests (from left to right are pristine $CsPbBr_3$ and PCC-IE-*n* (*n* = 1–4), respectively)). (b) Temporal evolution of PL intensity under heating at 70 °C for control sample and PCC-IE-*n* (*n* = 1–4). (c) Temporal evolution of PL intensity under UV light (365 nm) for control sample and PCC-IE-*n* (*n* = 1–4).

matrix. In these cyan/blue emitting composites, the strongly quantum confined $CsPbBr_3$ nanocrystals are effectively separated from each other by the polymeric networks, which are believed to impede thermal or photo induced ligand shedding, meantime inhibiting nanocrystal aggregation.

The favourable stability and high PLQY of the cyan/blue emitting $CsPbBr_3$ composites endow them good application potential in lighting and display fields. As a proof of concept, one of the composites, PCC-IE-2, was integrated to WLED excited by a blue chip (λ_{peak} = 455 nm). Another WLED without PCC-IE-2 was also assembled as the contrast device. As shown in Fig. 5(a), the electroluminescence (EL) spectrum of the WLED without PCC-IE-

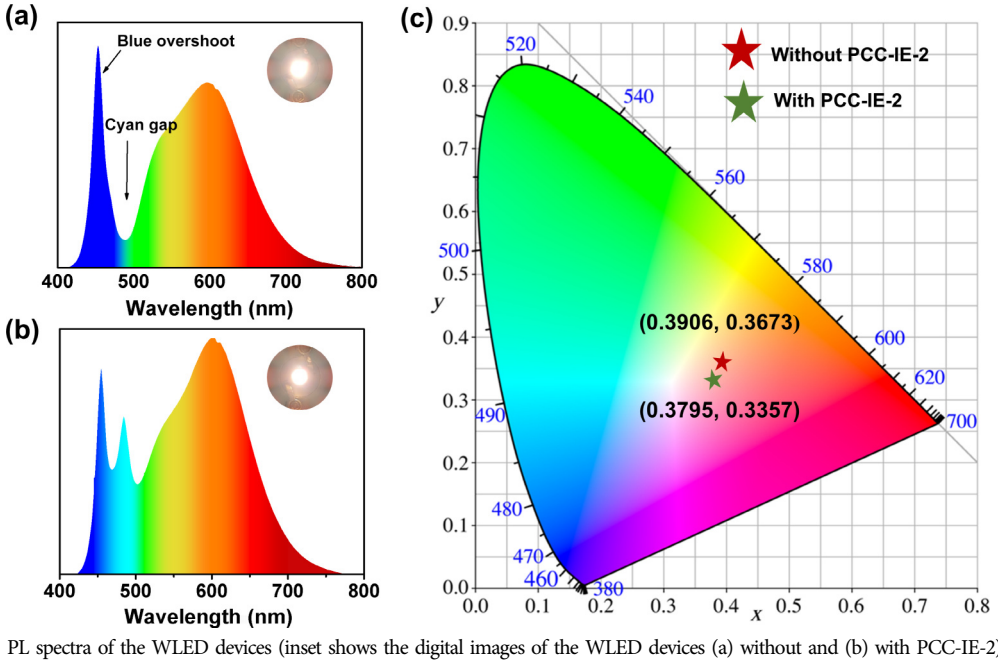

Figure 5 (a) and (b) PL spectra of the WLED devices (inset shows the digital images of the WLED devices (a) without and (b) with PCC-IE-2). (c) The CIE colour diagram of the WLED devices.

2 exhibits apparent cavity in the cyan region (470–520 nm) and excessive emission in the 440–460 nm range, namely "cyan gap" and "blue overshoot" [57], resulting in a relatively low color rendering index (Ra) of 77.7, a correlated color temperature (CCT) of 3606 K, and chromaticity coordinates of (0.3906, 0.3673). When PCC-IE-2 was incorporated, the "cyan gap" is efficiently made up, leading to prominent improvement of the Ra value to 86.4 (Fig. 5(b)). The corresponding WLED device presents a CCT of 3550 K and chromaticity coordinates of (0.3795, 0.3357) (Fig. 5(c)), lying in the warm white light region. These results demonstrate that the $CsPbBr_3$ composites have great application potential for full-spectrum lighting. Latest researches reported that cyan light is visually comfortable and beneficial to people's physical and mental health [58, 59]. Moreover, the cyan emitting $CsPbBr_3$ composites can absorb some redundant blue light, and decrease the overshoot from the blue chip at some extend, which is also conducive to the protection of retina.

3 Conclusion

In summary, we have demonstrated the successful preparation and stabilization of strongly quantum confined $CsPbBr_3$ NCs using APTES and PMHS through a post-synthetic chemical cutting and *in-situ* encapsulation method. By increasing the addition amount of APTES, the average size of the $CsPbBr_3$ NCs was tuned from 9.8 to 3.9 nm, resulting in a blue-shifted emission from 517 to 461 nm, along with a narrowed FWHM of approximately 15 nm. These strongly quantum confined $CsPbBr_3$ nanocrystals exhibited a PLQY greater than 80%, owing to defect passivation through A-site doping by the protonated APTES. The introduction of PMHS provided a protective barrier that prevented phase transformation of the $CsPbBr_3$ during the preparation process, while also *in situ* forming a polymeric encapsulation matrix, significantly enhancing the nanocrystals' tolerance to polar solvents. Notably, the resulting quantum-confined $CsPbBr_3$ composites PCC-IE-*n* (n = 1–4) retained over 70% of their initial PL intensity after aging at 70 °C or exposure to continuous 365 nm UV light (24 W) for 5 days. In contrast, the emission intensity of the pristine green-emitting $CsPbBr_3$ diminished by more than 90%, accompanied by a pronounced red shift in the PL peak under identical aging conditions. Furthermore, one of the composites, PCC-IE-2, was integrated to a WLED to alleviate the blue overshoot and compensate the cyan gap, which improves the Ra from 77.7 to 86.4. This work not only provides a facile strategy for preparation of strongly quantum confined $CsPbBr_3$ NCs with simultaneously high luminescent efficiency, exceptional color purity, and improved stability, but also advances their potential for practical applications in advanced light-emitting devices.

Electronic Supplementary Material: Supplementary material (experimental details, characterizations such as lifetime measurements, TEM images, EDX mapping images, FTIR spectra, XPS spectra, stability experiment, and XRD result) is available in the online version of this article at https://doi.org/10.26599/NR.2025.94907131.

Data availability

All data needed to support the conclusions in the paper are presented in the manuscript and the Electronic Supplementary Material. Additional data related to this paper may be requested from the corresponding author upon request.

Acknowledgements

This work was supported by the National Natural Science Foundation of China (Nos. 22109138 and 22178317).

Declaration of competing interest

All the contributing authors report no conflict of interests in this work.

Author contribution statement

H. Z.: Conceptualization, writing – original draft, writing – review & editing, funding acquisition. J. C.: Investigation, formal analysis, writing – original draft. T. T. Z.: Validation, formal analysis. R. W.: Investigation, formal analysis. X. M. W.: Investigation, formal analysis. X. J. X.: Writing – review & editing. J. L. W.: Conceptualization, validation, supervision, funding acquisition. All the authors have approved the final manuscript.

Use of AI statement

None.

References

[1] Kovalenko, M. V.; Protesescu, L.; Bodnarchuk, M. I. Properties and potential optoelectronic applications of lead halide perovskite nanocrystals. *Science* **2017**, *358*, 745–750.

[2] Jiang, G. C.; Erdem, O.; Hübner, R.; Georgi, M.; Wei, W.; Fan, X. L.; Wang, J.; Demir, H. V.; Gaponik, N. Mechanosynthesis of polymer-stabilized lead bromide perovskites: Insight into the formation and phase conversion of nanoparticles. *Nano Res.* **2021**, *14*, 1078–1086.

[3] Wang, H. R.; Zhang, X. Y.; Wu, Q. Q.; Cao, F.; Yang, D. W.; Shang, Y. Q.; Ning, Z. J.; Zhang, W.; Zheng, W. T.; Yan, Y. F. et al. Trifluoroacetate induced small-grained $CsPbBr_3$ perovskite films result in efficient and stable light-emitting devices. *Nat. Commun.* **2019**, *10*, 665.

[4] Zhuang, Z. C.; Li, Y. H.; Yu, R. H.; Xia, L. X.; Yang, J. R.; Lang, Z. Q.; Zhu, J. X.; Huang, J. Z.; Wang, J. O.; Wang, Y. et al. Reversely trapping atoms from a perovskite surface for high-performance and durable fuel cell cathodes. *Nat. Catal.* **2022**, *5*, 300–310.

[5] Yin, J.; Yang, H. Z.; Gutiérrez-Arzaluz, L.; Zhou, Y.; Brédas, J. L.; Bakr, O. M.; Mohammed, O. F. Luminescence and stability enhancement of inorganic perovskite nanocrystals via selective surface ligand binding. *ACS Nano* **2021**, *15*, 17998–18005.

[6] Pan, J.; Shang, Y. Q.; Yin, J.; De Bastiani, M.; Peng, W.; Dursun, I.; Sinatra, L.; El-Zohry, A. M.; Hedhili, M. N.; Emwas, A. H. et al. Bidentate ligand-passivated $CsPbI_3$ perovskite nanocrystals for stable near-unity photoluminescence quantum yield and efficient red light-emitting diodes. *J. Am. Chem. Soc.* **2018**, *140*, 562–565.

[7] Shen, Y. Y.; Tang, H. L.; Liu, F.; Lin, K. B.; Lu, J. X.; Yan, C. Z.; Feng, W. J.; Liu, K. K.; Wu, L. Q.; Li, M. J. et al. Stable cyan and white light-emitting diodes enabled by branched cations sterically stabilized 2D/3D perovskites. *Chem. Eng. J.* **2021**, *423*, 130160.

[8] Wu, Y.; Li, X. M.; Zeng, H. B. Highly luminescent and stable halide perovskite nanocrystals. *ACS Energy Lett.* **2019**, *4*, 673–681.

[9] Shen, Y. Y.; Yan, C. Z.; Lin, K. B.; Zhao, Y. P.; Xu, S. R.; Zhou, B.; Wei, Z. H.; Yan, K. Y. Recent advances on cyan-emitting ($480 \leq \lambda \leq 520$ nm) metal halide perovskite materials. *Small Sci.* **2021**, *1*, 2000077.

[10] Zhang, J. F.; Wang, L.; Zhang, X. Y.; Xie, G. H.; Jia, G. H.; Zhang, J. H.; Yang, X. Y. Blue light-emitting diodes based on halide

perovskites: Recent advances and strategies. *Mater. Today* **2021**, *51*, 222–246.

[11] Yoon, Y. J.; Shin, Y. S.; Jang, H.; Son, J. G.; Kim, J. W.; Park, C. B.; Yuk, D.; Seo, J.; Kim, G. H.; Kim, J. Y. Highly stable bulk perovskite for blue LEDs with anion-exchange method. *Nano Lett.* **2021**, *21*, 3473–3479.

[12] Wang, H. L.; Zhao, X. F.; Zhang, B. H.; Xie, Z. Y. Blue perovskite light-emitting diodes based on RbX-doped polycrystalline $CsPbBr_3$ perovskite films. *J. Mater. Chem. C* **2019**, *7*, 5596–5603.

[13] Zhuang, Z. C.; Li, Y.; Li, Y. H.; Huang, J. Z.; Wei, B.; Sun, R.; Ren, Y. J.; Ding, J.; Zhu, J. X.; Lang, Z. Q. et al. Atomically dispersed nonmagnetic electron traps improve oxygen reduction activity of perovskite oxides. *Energy Environ. Sci.* **2021**, *14*, 1016–1028.

[14] Vashishtha, P.; Ng, M.; Shivarudraiah, S. B.; Halpert, J. E. High efficiency blue and green light-emitting diodes using ruddlesden-popper inorganic mixed halide perovskites with butylammonium interlayers. *Chem. Mater.* **2019**, *31*, 83–89.

[15] Braly, I. L.; Stoddard, R. J.; Rajagopal, A.; Uhl, A. R.; Katahara, J. K.; Jen, A. K. Y.; Hillhouse, H. W. Current-induced phase segregation in mixed halide hybrid perovskites and its impact on two-terminal tandem solar cell design. *ACS Energy Lett.* **2017**, *2*, 1841–1847.

[16] Yang, H. W.; Feng, Y. Q.; Tu, Z. Y.; Su, K.; Fan, X. Z.; Liu, B. J.; Shi, Z. P.; Zhang, Y. Z.; Zhao, C. Y.; Zhang, B. Blue emitting $CsPbBr_3$ perovskite quantum dot inks obtained from sustained release tablets. *Nano Res.* **2019**, *12*, 3129–3134.

[17] Zhang, Y. D.; Sun, Y. J.; Wang, Q. Y.; Zhuang, Z. C.; Ma, Z. T.; Liu, L. M.; Wang, G. M.; Wang, D. S.; Zheng, X. S. Synergy of photogenerated electrons and holes toward efficient photocatalytic urea synthesis from CO_2 and N_2. *Angew. Chem., Int. Ed.* **2024**, *63*, e202405637.

[18] Kumar, S.; Jagielski, J.; Yakunin, S.; Rice, P.; Chiu, Y. C.; Wang, M. C.; Nedelcu, G.; Kim, Y.; Lin, S. C.; Santos, E. J. G. et al. Efficient blue electroluminescence using quantum-confined two-dimensional perovskites. *ACS Nano* **2016**, *10*, 9720–9729.

[19] Zhao, J. Y.; Cao, S. N.; Li, Z.; Ma, N. Amino acid-mediated synthesis of $CsPbBr_3$ perovskite nanoplatelets with tunable thickness and optical properties. *Chem. Mater.* **2018**, *30*, 6737–6743.

[20] Bekenstein, Y.; Koscher, B. A.; Eaton, S. W.; Yang, P. D.; Alivisatos, A. P. Highly luminescent colloidal nanoplates of perovskite cesium lead halide and their oriented assemblies. *J. Am. Chem. Soc.* **2015**, *137*, 16008–16011.

[21] Dong, Y. T.; Qiao, T.; Kim, D.; Parobek, D.; Rossi, D.; Son, D. H. Precise control of quantum confinement in cesium lead halide perovskite quantum dots via thermodynamic equilibrium. *Nano Lett.* **2018**, *18*, 3716–3722.

[22] Lin, H.; Wei, Q.; Ng, K. W.; Dong, J. Y.; Li, J. L.; Liu, W. W.; Yan, S. S.; Chen, S.; Xing, G. C.; Tang, X. S. et al. Stable and efficient blue-emitting $CsPbBr_3$ nanoplatelets with potassium bromide surface passivation. *Small* **2021**, *17*, 2101359.

[23] Li, J.; Gan, L.; Fang, Z. S.; He, H. P.; Ye, Z. Z. Bright tail states in blue-emitting ultrasmall perovskite quantum dots. *J. Phys. Chem. Lett.* **2017**, *8*, 6002–6008.

[24] Xiang, Q. Y.; Zhou, B. Z.; Cao, K.; Wen, Y. W.; Li, Y.; Wang, Z. J.; Jiang, C. C.; Shan, B.; Chen, R. Bottom up stabilization of $CsPbBr_3$ quantum dots-silica sphere with selective surface passivation via atomic layer deposition. *Chem. Mater.* **2018**, *30*, 8486–8494.

[25] Zhang, Q.; Jiang, M. H.; Yan, G. J.; Feng, Y. Q.; Zhang, B. Surface ligand engineering involving fluorophenethyl ammonium for stable and strong emission $CsPbBr_3$ quantum dots and high-performance QLEDs. *J. Mater. Chem. C* **2022**, *10*, 5849–5855.

[26] Fan, C.; Liu, H. P.; Zhou, J. W.; Dai, X. L.; He, H. P.; Ye, Z. Z. Ultrastable and highly efficient $CsPbBr_3$ composites achieved by dual-matrix encapsulation for display devices. *InfoMat* **2023**, *5*, e12417.

[27] Li, X. Y.; Zhuang, Z. C.; Chai, J.; Shao, R. W.; Wang, J. H.; Jiang, Z. L.; Zhu, S. W.; Gu, H. F.; Zhang, J.; Ma, Z. T. et al. Atomically strained metal sites for highly efficient and selective photooxidation. *Nano Lett.* **2023**, *23*, 2905–2914.

[28] Xiao, H.; Wei, Y.; Dang, P. P.; Liang, S.; Cheng, Z. Y.; Li, G. G.; Lin, J. Polymer ligands induced remarkable spectral shifts in all-inorganic lead halide perovskite nanocrystals. *J. Mater. Chem. C* **2020**, *8*, 9968–9974.

[29] Takhellambam, D.; Meena, T. R.; Jana, D. Room temperature synthesis of blue and green emitting $CsPbBr_3$ perovskite nanocrystals confined in mesoporous alumina film. *Chem. Commun.* **2019**, *55*, 4785–4788.

[30] Malgras, V.; Henzie, J.; Takei, T.; Yamauchi, Y. Stable blue luminescent $CsPbBr_3$ perovskite nanocrystals confined in mesoporous thin films. *Angew. Chem., Int. Ed.* **2018**, *57*, 8881–8885.

[31] Zhang, H. Y.; Wang, B. L.; Niu, Z. J.; Chen, G. R.; Guan, B. Y.; Li, J. Y.; Yu, J. H. Ultrasmall water-stable $CsPbBr_3$ quantum dots with high intensity blue emission enabled by zeolite confinement engineering. *Mater. Horiz* **2023**, *10*, 5079–5086.

[32] Yoon, S.; Seo, M.; Kim, I. S.; Lee, K.; Woo, K. Ultra-stable and highly efficient white light emitting diodes through $CsPbBr_3$ perovskite nanocrystals-silica composite phosphor functionalized with surface phenyl molecules. *Small* **2023**, *19*, 2206311.

[33] Shamsi, J.; Urban, A. S.; Imran, M.; De Trizio, L.; Manna, L. Metal halide perovskite nanocrystals: Synthesis, post-synthesis modifications, and their optical properties. *Chem. Rev.* **2019**, *119*, 3296–3348.

[34] Huang, H.; Zhao, W. R.; Yang, H. X.; Zhang, X. L.; Su, J. N.; Hu, K. G.; Nie, Z. G.; Li, Y.; Zhong, J. Y. *In situ* synthesis of blue-emitting bromide-based perovskite nanoplatelets towards unity quantum efficiency and ultrahigh stability. *J. Mater. Chem. C* **2021**, *9*, 5535–5543.

[35] González-Pedro, V.; Veldhuis, S. A.; Begum, R.; Bañuls, M. J.; Bruno, A.; Mathews, N.; Mhaisalkar, S.; Maquieira, Á. Recovery of shallow charge-trapping defects in $CsPbX_3$ nanocrystals through specific binding and encapsulation with amino functionalized silanes. *ACS Energy Lett.* **2018**, *3*, 1409–1414.

[36] De Roo, J.; Ibáñez, M.; Geiregat, P.; Nedelcu, G.; Walravens, W.; Maes, J.; Martins, J. C.; Van Driessche, I.; Kovalenko, M. V.; Hens, Z. Highly dynamic ligand binding and light absorption coefficient of cesium lead bromide perovskite nanocrystals. *ACS Nano* **2016**, *10*, 2071–2081.

[37] Ding, H. W.; Jiang, H.; Wang, X. M. How organic ligands affect the phase transition and fluorescent stability of perovskite nanocrystals. *J. Mater. Chem. C* **2020**, *8*, 8999–9004.

[38] Sun, C.; Zhang, Y.; Ruan, C.; Yin, C. Y.; Wang, X. Y.; Wang, Y. D.; Yu, W W. Efficient and stable white LEDs with silica-coated inorganic perovskite quantum dots. *Adv. Mater.* **2016**, *28*, 10088–10094.

[39] Huang, S. Q.; Li, Z. C.; Kong, L.; Zhu, N. W.; Shan, A. D.; Li, L. Enhancing the stability of $CH_3NH_3PbBr_3$ quantum dots by embedding in silica spheres derived from tetramethyl orthosilicate in "waterless" toluene. *J. Am. Chem. Soc.* **2016**, *138*, 5749–5752.

[40] Zhou, J.; Fang, F.; Chen, W.; Mei, M.; Liu, P. Z.; Hao, J. J.; Tang, H. D.; Liang, S. Z.; Lei, W.; Pan, R. K. et al. Luminescent perovskite nanocrystal composites via *in situ* ligand polymerization towards display applications. *J. Mater. Chem. C* **2021**, *9*, 14740–14748.

[41] Choi, J. W.; Woo, H. C.; Huang, X. G.; Jung, W. G.; Kim, B. J.; Jeon, S. W.; Yim, S. Y.; Lee, J. S.; Lee, C. L. Organic–inorganic hybrid perovskite quantum dots with high PLQY and enhanced carrier mobility through crystallinity control by solvent engineering and solid-state ligand exchange. *Nanoscale* **2018**, *10*, 13356–13367.

[42] Xu, Y. Q.; Hu, X. B.; Tang, H. D.; Hu, Q.; Wang, S. H.; Chen, T.; Zhang, X. J.; Jiang, W. H.; Wang, L. J.; Jiang, W. Highly efficient silica coated perovskite nanocrystals with the assistance of ionic liquids for warm white LEDs. *Nanoscale* **2023**, *15*, 631–643.

[43] Liu, Q. B.; Liu, C.; Zhou, H. A study on the epitaxial large-size $CsPbBr_3$ nanosheets grown by vapor phase epitaxy. *Appl. Phys. A* **2023**, *129*, 242.

[44] Ye, C. Y.; Zhou, Y. J.; Ge, J.; Zhang, Q. Mechanistic insights into the photoluminescence enhancement in surface ligand modified $CsPbBr_3$ perovskite nanocrystals. *J. Phys. Chem. Lett.* **2024**, *15*, 226–233.

[45] Wang, S. J.; Chen, D. J.; Xu, K. Y.; Hu, J.; Huang, D. C.; Hong, M. C.; Zhu, H. M. Organic polystyrene and inorganic silica double shell protected lead halide perovskite nanocrystals with high emission efficiency and superior stability. *Nano Res.* **2023**, *16*, 10507–10514.

[46] Song, W. T.; Wang, Y. M.; Wang, B.; Yao, Y. F.; Wang, W. G.; Wu, J. H.; Shen, Q.; Luo, W. J.; Zou, Z. G. Super stable $CsPbBr_3@SiO_2$ tumor imaging reagent by stress-response encapsulation. *Nano Res.* **2020**, *13*, 795–801.

[47] Trinh, C. K.; Lee, H.; So, M. G.; Lee, C. L. Synthesis of chemically stable ultrathin SiO_2-coated core-shell perovskite QDs via modulation of ligand binding energy for all-solution-processed light-emitting diodes. *ACS Appl. Mater. Interfaces* **2021**, *13*, 29798–29808.

[48] Wang, L. L.; Liu, H.; Zhang, Y. H.; Mohammed, O. F. Photoluminescence origin of zero-dimensional Cs_4PbBr_6 perovskite. *ACS Energy Lett.* **2020**, *5*, 87–99.

[49] Ma, C.; Zhang, M. Y.; Zhang, J. R.; Liao, J. F.; Sun, H.; Ji, D. X.; Pang, R. X.; Zhang, H.; Liu, J. W.; Liu, S. Z. Highly luminescent and stable perovskite quantum dots films for light-emitting devices and information encryption. *Adv. Funct. Mater.* **2024**, *34*, 2316717.

[50] Wang, A. F.; Liu, J. X.; Li, J. J.; Cheng, S. W.; Zhang, Y. P.; Wang, Y. C.; Xie, Y.; Yu, C.; Chu, Y.; Dong, J. J. et al. Dendrimer-encapsulated halide perovskite nanocrystals for self-powered white light-emitting glass. *J. Am. Chem. Soc.* **2023**, *145*, 28156–28165.

[51] Xia, J. K.; Xu, J. W.; Yu, B.; Liang, X.; Qiu, Z.; Li, H.; Feng, H. J.; Li, Y. F.; Cai, Y. J.; Wei, H. Y. et al. A metal-sulfur-carbon catalyst mimicking the two-component architecture of nitrogenase. *Angew. Chem., Int. Ed.* **2024**, *63*, e202412740.

[52] Jiang, S. Q.; Sui, H. J.; He, B. L.; Zhang, X. Y.; Zong, Z. H.; Chen, H. Y.; Tang, Q. W. Synergistic effect of alkali metal doping and thiocyanate passivation in $CsPbBr_3$ for HTM-free all-inorganic perovskite solar cells. *Dalton Trans.* **2023**, *52*, 9772–9779.

[53] Dong, H. R.; Zhao, H. Y.; Xuan, T. T.; Bai, W. H.; Lin, T. Y.; Cai, Y. X.; Xie, R. J. Constructing perovskite/polymer core/shell nanocrystals with simultaneous high efficiency and stability for mini-LED backlights. *ACS Appl. Mater. Interfaces* **2023**, *15*, 29297–29307.

[54] Geng, Y. H.; Guo, J. Z.; Wang, H. Q.; Ling, S. D.; Chen, Z.; Chen, S.; Xu, J. H. Large-scale production of ligand-engineered robust lead halide perovskite nanocrystals by a droplet-based microreactor system. *Small* **2022**, *18*, 2200740.

[55] Ye, J. Z.; Byranvand, M. M.; Martínez, C. O.; Hoye, R. L. Z.; Saliba, M.; Polavarapu, L. Defect passivation in lead-halide perovskite nanocrystals and thin films: Toward efficient LEDs and solar cells. *Angew. Chem., Int. Ed.* **2021**, *60*, 21636–21660.

[56] Chen, J. S.; Liu, D. Z.; Al-Marri, M. J.; Nuuttila, L.; Lehtivuori, H.; Zheng, K. B. Photo-stability of $CsPbBr_3$ perovskite quantum dots for optoelectronic application. *Sci. China Mater.* **2016**, *59*, 719–727.

[57] Peng, M.; Sun, S. B.; Xu, B.; Deng, Z. T. Polymer-encapsulated halide perovskite color converters to overcome blue overshoot and cyan gap of white light-emitting diodes. *Adv. Funct. Mater.* **2023**, *33*, 2300583.

[58] Zhang, H. D.; Lv, Y.; Chang, Y. L.; Guo, X. Y.; Zou, D. Y.; Sun, Y. F.; Zeng, Q. H.; Liu, X. Y. Ultra-small-size, highly efficient and stable $CsPbBr_3$ quantum dots synthesized by using a cesium-dodecyl benzene sulfonic acid solution. *Chem. Eng. J.* **2023**, *473*, 145213.

[59] He, X. Y.; Li, T. F.; Liang, Z. F.; Liu, R. M.; Ran, X.; Wang, X. J.; Guo, L. J.; Pan, C. F. Enhanced cyan photoluminescence and stability of $CsPbBr_3$ quantum dots via surface engineering for white light-emitting diodes. *Adv. Optical Mater.* **2024**, *12*, 2302726.